



PAPER

View Article Online
View Journal | View Issue



Cite this: *Environ. Sci.: Adv.*, 2024, 3, 10

Superior single- and multi-component siloxane removal from water using a faulted silica DON zeolite adsorbent†

Dariana R. Vega-Santander, Rodinson Arrieta-Pérez, Daniela Rivera-Mirabal, Gabriela Del Valle-Pérez, Miguel Sepúlveda-Pagán, Juan C. Muñoz-Senmache, Yomaira J. Pagán-Torres  and Arturo J. Hernández-Maldonado *

Removal of monomeric siloxanes from water *via* adsorption poses a significant challenge, particularly during water reclamation in closed-volume systems. In this study, both faulted and faultless variants UTD-1 pure silica zeolites with a DON-type framework were considered for the removal of monomethylsilanetriol (MMST), dimethylsilanediol (DMSD), and trimethylsilanol (TMS), in single- and multi-component fashion. The results showed that UTD-1_{faulted} exhibited the largest adsorption capacity for TMS, with a maximum adsorption uptake of 73.1 mg g⁻¹ in the 1 to 140 mg L⁻¹ aqueous concentration range. This is 7× larger than UTD-1_{faultless} and at least one magnitude larger than other materials such as activated carbon. The interaction of TMS with UTD-1_{faulted} is mainly with OH groups from siloxy-related faults present in the material, and multicomponent adsorption tests showed that TMS helps to drive the uptake of other siloxanes *via* co-adsorption. UTD-1 is a promising material platform for developing adsorption-based strategies for removing persistent monomeric siloxanes from aqueous environments.

Received 14th September 2023
Accepted 9th November 2023

DOI: 10.1039/d3va00282a

rsc.li/esadvances

Environmental significance

Linear siloxanes are ubiquitous and may enter water sources, with some being capable of affecting the human central nervous system upon ingestion. In closed-volume systems, where water reclamation is perhaps mandatory, their concentration is much more prominent due to the intrinsic infrastructure. Existing commercial adsorbents lack capacity and selectivity toward linear siloxanes, particularly when in mixtures. Given that adsorption is amongst the separation platforms with smaller energy requirement footprints, developing adsorbent materials with siloxane selectivity and capacity would be ideal. Pure porous silica zeolites with framework surface faults, in the form of siloxy groups, are not only selective toward individual or single-component siloxanes for removal from water but also multi-component matrices.

Introduction

Siloxanes are a category of silicone derivatives containing Si–O bonding¹ arranged in linear or cyclic structures, extensively employed across multiple industries and consumer products.^{2–4} In 2020, the total worldwide production of silicon-based compounds was around eight million metric tons,⁵ and production will continue to grow in the coming years.^{6,7} Consequently, the concentration of siloxane compounds that could be released into the environment will also increase, and siloxanes are already detected in water, soil, air, and sediments.^{8–16} This also poses a potential risk to the environment and human health since some siloxanes are known to be

toxic, particularly those with low molecular weight. Linear siloxanes that have been detected in water and that are products of the hydrolysis of larger siloxanes include monomethylsilanetriol (MMST),¹⁷ dimethylsilanediol (DMSD), and trimethylsilanol (TMS).^{18,19} DMSD is toxic to humans if ingested for long periods, even at low concentrations (*i.e.*, mg L⁻¹),²⁰ while TMS has been associated with causing central nervous system problems.²¹ Such toxicity arises from the ability of the siloxane to permeate biological membranes and skin layers.²² Although MMST is used in dietary supplements, it is found in the environment in combination with DMSD and TMS since all are usually produced simultaneously during the hydrolysis of larger siloxanes. For instance, MMST, TMS, and DMSD have been detected in reclaimed water from closed-volume environments, such as the International Space Station (ISS); low molecular weight siloxane concentrations up to 10 mg L⁻¹ have been reported downstream in the ISS.^{19,23,24}

Department of Chemical Engineering, University of Puerto Rico, Mayagüez Campus, Mayagüez, PR 00681, USA. E-mail: arturoj.hernandez@upr.edu

† Electronic supplementary information (ESI) available. See DOI: <https://doi.org/10.1039/d3va00282a>



Developing appropriate adsorbents could be an efficient and cost-effective solution for siloxane removal.²⁵ The United States National Aeronautics and Space Administration (NASA) has already focused on the usage of commercial adsorbents such as ion exchange resins^{23,26} and activated carbon;^{27–30} for instance, NASA has reported siloxane uptake capacities for TMS and DMSD of approximately 0.15 and 0.30 mg per cm³ of adsorbent, respectively.¹⁹ More recently, Hernández-Maldonado and co-workers³¹ prepared a hierarchical zeolite–carbon composite *via* confined space synthesis and reported adsorption capacities for TMS and DMSD of around 2.0 and 0.8 mg cm^{−3}, respectively, highlighting the importance of adding specific adsorbent–adsorbate interactions to the overall surface potential as well as hydrophobicity to increase selectivity toward the siloxane and uptake capacities.

Pure silica zeolite materials (PSZs), which contain only silicon and oxygen atoms, are highly hydrophobic^{32,33} and this holds significant importance for water treatment applications.^{34–37} Moreover, PSZs display exceptional high thermal stability, opening the possibility of being regenerated by thermal swing after being spent during adsorption.^{38,39} PSZs have been extensively tested as adsorbents for gas/vapor^{40–43} and liquid^{38,44–46} phase separations. For the latter, PSZs have even been considered for removing several micropollutants from water in computational studies by Chen *et al.*,⁴⁷ who showed the importance of pore diameters, surface areas, and crystal frameworks for the uptake of different problematic compounds. Although it is difficult to tailor extraframework moieties that act as specific adsorption sites in PSZs, exploiting silanol groups resulting from structural defects is an alternative. The presence or absence of these could significantly impact the PSZ material surface potential and its performance in adsorption and catalysis applications.^{48–50} Further, combining such defects with a larger pore channel could make PSZ an excellent alternative to achieve sound diffusion of adsorbates and high capacity, essential for continuous or dynamic adsorption scenarios. UTD-1 (University of Texas at Dallas, number 1) is a PSZ with a DON-type framework with pores bounded by 14 tetrahedral atoms, the first PSZ with extra-large pores with a diameter of approximately 10 × 7.5 Å.^{51,52} UTD-1 can exhibit structural defects or faults that cause silanol groups in its structure, which are formed to compensate for the positive charge of the structure-directing agent (SDA) used during the synthesis process. In turn, the silanol groups could act as active sites for the adsorption of target molecules, and the size of the UTD-1 pores enables a high selectivity in capturing molecules overtaking diffusion problems encountered in other zeolite types. UTD-1 has about 3.5% faults per unit cell, amongst the largest reported for a PSZ, and all are exposed to the pore surface.⁵² For instance, many of the surface faults of pure silica MFI are in positions that are sterically forbidden for interactions with guest molecules (*i.e.*, not near the main pore).⁵³

The main goal of this work is to evaluate the effect of structural faults in UTD-1 zeolite on the removal of monomeric siloxanes (MMST, DMSD, and TMS) from water in single- and multi-component fashion. To achieve this, faulted and faultless UTD-1 frameworks (*i.e.*, UTD-1_{faulted} and UTD-1_{faultless}) were

synthesized *via* hydrothermal methods following or modifying recipes published by Freyhardt *et al.*⁵¹ and Wessels *et al.*,⁴⁹ respectively. The resulting adsorbent materials were fully characterized *via* X-ray diffraction (XRD), nitrogen porosimetry, thermogravimetric analysis (TGA), water contact angle measurements, zeta potential analysis, and Fourier transform infrared (FT-IR) spectroscopy. FT-IR was also used in an attempt to elucidate adsorption mechanisms. Finally, multi-cycle adsorption studies with thermal-assisted and OH-replenishment treatments were performed to evaluate the possibility of regeneration of faulted UTD-1 adsorbents.

Experimental

Two UTD-1 variants were synthesized following methods reported elsewhere.⁵⁴ UTD-1_{faulted} was synthesized in hydroxide media, following the procedure outlined by Freyhardt *et al.*,⁵¹ while UTD-1_{faultless} was prepared according to the method reported by Wessels *et al.*⁴⁹ in fluoride media. The synthesis of both UTD-1 variants involved the use of bis(pentamethylcyclopentadienyl)cobalt(III) hydroxide ([Cp*]₂Co)OH) as SDA, which was effectively produced with a modification of a previously reported method.⁵⁴ Both faulted and faultless variants of UTD-1 were fully characterized to assess their crystallinity, textural properties, thermal stability, and hydrophobicity, among others. The adsorption capacities for MMST, DMSD, and TMS were evaluated under both single and multicomponent conditions. Detailed information on reagents, synthesis procedures, characterization, and adsorption protocols, including adsorption regeneration tests, can be found in the ESI text.†

Results and discussion

Synthesis and characterization of UTD-1 adsorbents

PSZs consist of silicon and oxygen atoms and are hydrophobic without acid sites. Thus, the competitive adsorption of metal cations in water treatment applications can be significantly reduced.⁵⁸ Two DON-type PSZ adsorbent materials were prepared here using [Cp*]₂Co)OH as the SDA.⁵¹ One of these DON PSZ was prepared with framework faults or siloxy groups in its structure (UTD-1_{faulted}) to counterbalance the structural charges from the organometallic complex of the SDA.⁵² Subsequently, these siloxy groups give rise to silanol groups during the decomposition of the SDA; the elimination of the SDA is essential to fully expose the material porosity. The other DON-type material (UTD-1_{faultless}) was made in a fluorine medium to eliminate faults since, in this case, fluoride ions can counterbalance the positive charge of the SDA.^{49,51,52,59,60} The crystallinity and the DON topology of the adsorbents were corroborated *via* XRD. The XRD profiles shown in Fig. 1 are consistent with the previously reported XRD profiles of a fully detemplated DON-type zeolite.^{49,52,61} It should be noted that the presence of expected structural faults in UTD-1_{faulted} will not be readily apparent from crystallographic measurements as these are highly dispersed along the long range of the one-dimensional 14-ring channel, locally impacting the structure but not the long-range order or the dimension of the pores.^{49,59}



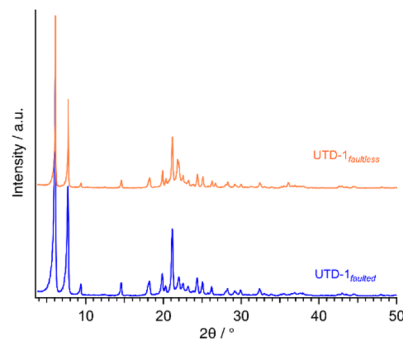


Fig. 1 Powder X-ray diffraction patterns for detemplated UTD-1 (DON) variants.

In fact, Lobo *et al.* employed solid-state nuclear magnetic resonance (NMR) spectroscopy and simulations of intergrowth structures with the program DiFFAX to elucidate the level of faulting in these materials.⁵⁹ As shown below, the present work used TGA and FTIR data to quantify the siloxy groups directly associated with the faults (*i.e.*, source of specific OH).

TGA data showed that both UTD-1 variants are thermally stable up to *ca.* 900 °C. The level of hydrophobicity of both UTD-1 materials is apparent in the TGA data gathered, and it was also corroborated *via* contact angle measurements (see Fig. 2). The higher water content of UTD-1_faulted compared to UTD-1_faultless could be related to the interaction of water molecules with silanol groups from the faults in the former. However, both materials still exhibit considerable hydrophobicity, which confers an advantageous trait for adsorption processes in aqueous environments by eliminating competition between target contaminants and water molecules for the available active adsorption sites.

UTD-1_faultless exhibits a weight loss within the range of 175 to 300 °C, which could be attributed to the thermal decomposition and elimination of residual traces of fluorine introduced during the synthesis process.^{62,63} Both DON-type materials exhibited a weight loss within the range of 470 to 750 °C, which could be attributed to the condensation of silanol groups⁴⁸ that emerge during the removal of the SDA^{49,52} and that condense at high temperatures. Based on reports for other PSZ materials also

synthesized in a fluorinated medium,^{50,64} therefore, it can be inferred that UTD-1_faultless also contains a certain amount of silanol groups.

Silanols are localized either on the external surface or within the structure of the zeolite,^{48,49,52,60} and can exist in various forms in zeolites, including isolated silanol, geminal silanol, and silanol nest, among others.^{48,65} In the case of UTD-1_faultless, the broad peak observed in the weight loss derivative profile indicates a wide variety of silanol groups in the structure. For UTD-1_faulted, the peak maximum centered at 550 °C showed a high population of a specific type of silanol group. This region is likely associated with siloxy $\text{SiO}^- \cdots \text{HOSi}$ groups (*i.e.*, geminal silanol or silanol nest); condensation occurs when these silanol groups are in proximity, producing water.^{48,60} A deconvolution of the weight derivative with respect to temperature for UTD-1_faulted in the region between 470 and 750 °C (see Fig. S1†), conducted to identify the temperature range and the area of the peak with a maximum at 550 °C, showed that the material has a weight loss of approximately 0.5% wt (range is 470–675 °C; deconvolution region with 67% area) when correlated to the corresponding location within the TGA weight loss profile (Fig. 2). This weight loss probably corresponds solely to the release of water during the condensation of a population of silanol groups present only in UTD-1_faulted. Considering that for every two silanol groups that condense, one water molecule is formed, the weight percentage corresponding to this water content (*i.e.*, 0.5 wt%) indicates the presence of a population of 2.1 OH sites per UTD-1 unit cell. This value agrees with those previously reported by Lobo *et al.*⁵² based on solid-state NMR spectroscopy studies, showing a population of these species accounted for 3.5% of the total silicon in the structure (*i.e.*, 2.2 OH sites per DON unit cell).⁵²

Upon full detemplation, both UTD-1 variants showcase type I nitrogen adsorption isotherm profiles (−196 °C; Fig. S2†) as defined by the IUPAC (International Union of Pure and Applied Chemistry), characteristic of micropore materials. However, the overall N_2 adsorption uptake capacity is larger in the case of UTD-1_faulted and this might be due to access of N_2 to voids resulting from the previously discussed faults. In fact, BET surface areas are around 326 and 290 $\text{m}^2 \text{g}^{-1}$ for UTD-1_faulted and UTD-1_faultless, respectively. Furthermore, although the pore size distribution (PSD) profiles for both materials show an average pore size of *ca.* 10 Å (see Fig. S3†), a notable discrepancy can be observed when comparing the areas under the said profiles; the area under a PSD yields the pore volume of a material. The pore volume for UTD-1_faultless is *ca.* 0.135 $\text{cm}^3 \text{g}^{-1}$. In the case of UTD-1_faulted, the area is *ca.* 0.165 $\text{cm}^3 \text{g}^{-1}$, which also suggests that N_2 is accessing additional voids compared to the faultless variant.

Given that the PSD profile for UTD-1_faulted appears asymmetrical, a deconvolution was made, and the analysis yielded what seems to be two pore populations (refer to Fig. S4†). Determining the area under the curve for the most prominent peak reveals that UTD-1_faulted possesses primary pores with a volume of around 0.135 $\text{cm}^3 \text{g}^{-1}$, equivalent to UTD-1_faultless. Meanwhile, the second pore population (smallest peak) exhibits a pore volume of roughly 0.03 $\text{cm}^3 \text{g}^{-1}$. This suggests that at

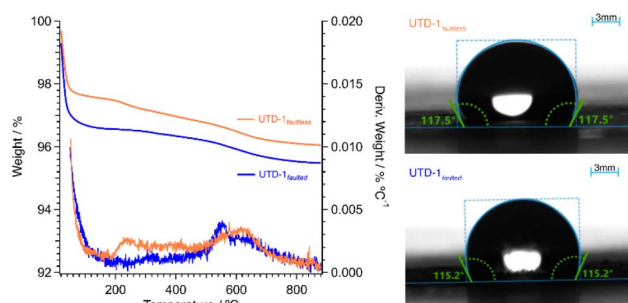


Fig. 2 (Left) Thermal gravimetric profiles for detemplated UTD-1 variants. Data gathered under air atmosphere. (Right) Water contact angle measurements for UTD-variants.



least a portion of the voids produced by the faults are indeed accessible to N_2 adsorbate molecules.

Finally, both UTD-1 variants were also analyzed to estimate the effective surface charges *via* zeta potential analysis. The profiles shown in Fig. 3 indicate that both variants have a negatively charged surface throughout most of the pH range, with an isoelectric point of around 4. These data will be employed throughout the discussion of the adsorption of siloxanes.

Single component adsorption

Fig. 4 displays the single component isotherms gathered for the adsorption of MMST, DMSD, or TMS onto UTD-1 at pH ~ 7 and ambient temperature. The data were fitted with the modified Dubinin–Astakhov isotherm model (MDA), and the saturation loadings were estimated under the assumption of full occupancy of the pore by densely packed adsorbates, wherein siloxanes molecules behave as spheres and fill perfectly within the adsorbent pore. The corresponding model parameters (see Table S1†) were determined using non-linear regression, and their suitability was assessed by computing the residual root mean square errors (RRMSE).

The maximum MMST adsorption loadings for UTD-1_{faulted} and UTD-1_{faultless} were 5.7 and 0.8 mg g⁻¹. Given that MMST is highly hydrophilic ($\log K_{OW} = -0.41$, Table 1) and has a strong tendency to self-condense,^{31,55} its preference for adsorbate–adsorbate interactions and its affinity for water would explain the lower interaction with both UTD-1 adsorbent variants, compared to TMS. However, the faulted material exhibits an MMST adsorption capacity approximately seven times greater relative to UTD-1_{faultless}. The adsorbate–adsorbent interaction is likely attributed to the hydroxyl groups of the MMST molecule and the silanol groups resulting from the imperfections in UTD-1_{faulted}. In the case of the DMSD, the adsorption loading was more significant compared to MMST, with UTD-1_{faulted} and UTD-1_{faultless} achieving loading values of 12 and 15 mg g⁻¹, respectively. The zeta potential results (Fig. 3) indicate that both UTD-1 variants possess significant negative surface charge profiles. Considering that DMSD contains positive regions due to its two methyl groups, it is plausible to suggest that the interaction between DMSD and the highly negative adsorbent surfaces primarily occurs through electrostatic interactions.

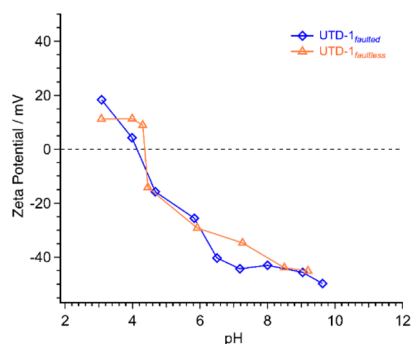


Fig. 3 Zeta potential measurements for UTD-1 materials.

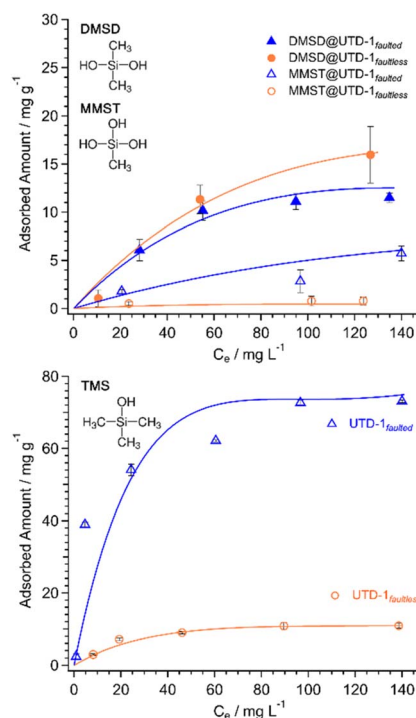


Fig. 4 Single component equilibrium adsorption isotherms for (top) MMST and DMSD, and (bottom) TMS onto UTD-1. Conditions: ambient temperature and pH ~ 7 . Data includes error bars.

The slightly superior adsorption capacity of UTD-1_{faultless} for DMSD can be attributed to the material's hydrophobic nature. Although both UTD-1 variants exhibit hydrophobic characteristics, as indicated by the water contact angle measurements, the thermogravimetric analysis reveals that UTD-1_{faulted} does adsorb more water than the faultless variant (see Fig. 2). This increased water adsorption influences the DMSD adsorption capacity of the faulted variant, resulting in a somewhat reduced capacity for DMSD adsorption. Moreover, if the physical and chemical properties of DMSD and MMST are compared, it is observed that they are quite similar (Table 1), with the former being slightly more stable because of the three hydroxyl groups; this renders MMST more susceptible to self-condensation,⁵⁵ thereby leading to the possibility of less interaction with the adsorbent surface. The interactions are evidenced in values of the MDA model C parameter (see Table S1†), which is inversely related to the adsorption energy (ESI eqn (S2)†). Due to the weaker interaction between both adsorbent variants and MMST, the C parameter values are larger compared to DMSD, almost by an order of magnitude.

For TMS, the observed maximum adsorption loadings were 73.1 and 10.8 mg g⁻¹ for UTD-1_{faulted} and UTD-1_{faultless}, respectively (Fig. 4). Although both materials have the same framework topology (*i.e.*, DON) and almost identical textural characteristics, it is remarkable that the shape of the TMS adsorption isotherm in the case of UTD-1_{faulted} is quite rectangular, suggesting the presence of significant, specific interactions between the corresponding adsorption sites and the TMS, even at equilibrium concentrations below 10 mg L⁻¹. The



Table 1 Physicochemical properties of MMST, DMSD, and TMS

	Monomethylsilanetriol (MMST)	Dimethylsilanediol (DMSD)	Trimethylsilanol (TMS)
pK_a ⁵⁵	10.75	11.90	11.00
$\log K_{ow}$ ^{55–57}	−0.87	−0.41	1.14
Molecular weight (g mol ^{−1})	94.14	92.17	90.20
Kinetic diameter (Å) ⁴⁷	4.30	4.34	4.55
Water solubility (g L ^{−1}) ⁵⁵	>2000.00	2450.00	42.6
Boiling point (°C) ⁵⁵	201.00	100.35	99.00

presence of OH groups in silica-rich surfaces is known to enhance the uptake of siloxanes significantly but from head-space biogas.⁶⁶ Therefore, given that UTD-1_{faulted} possess OH groups that counterbalance structural charges as a result of detemplation, it is plausible that these species are also serving as specific adsorption sites during the uptake of siloxanes from water; specifically in the TMS uptake.

As mentioned during the materials characterization discussion, the population of siloxy-related silanol groups in UTD-1_{faulted} is about 2.1 OH sites per unit cell. The maximum observed adsorption uptake of TMS is *ca.* 73.1 mg of TMS per g of UTD-1_{faulted} or about 3 TMS molecules per UTD-1_{faulted} unit cell (Fig. 4), and this strongly suggests preferential adsorption of TMS at the silanol group sites. However, it should be noted that UTD-1_{faultless} also possesses a surface capable of undergoing interaction with TMS. Akin to the scenario observed during DMSD adsorption, such interaction may arise from nonspecific adsorbate–adsorbent interactions as opposed to what is probably happening in the faulted variant. This can be corroborated by the comparable adsorption capacities that both UTD-1 variants exhibited toward DMSD and MMST (Fig. 4 (top)).

In general, the superior adsorption performance of UTD-1 materials is prominently due to the level of hydrophobicity of its silica-rich framework (*i.e.*, PSZ). And in the case of UTD-1_{faulted}, the performance is also due to the existence of sites for specific interactions. The adsorption capacity of UTD-1_{faulted} for TMS and DMSD contaminants is at least two orders of magnitude higher than that of commercially available adsorbent materials or even the zeolite–carbon composites previously tested for the removal of these contaminants at equilibrium concentrations around 10 mg L^{−1} (see Table S2†).^{19,31}

Mechanism for TMS single component adsorption

Since TMS was the adsorbate with the highest affinity toward UTD-1, an FTIR analysis was developed to elucidate the possible adsorption mechanisms. Fig. S5† gathers FTIR spectra for both UTD-1 variants after detemplation, where two broad IR bands related to the framework Si–O–Si and Si–O are located between 750–850 cm^{−1} and 1000–1300 cm^{−1}. A band at 950 cm^{−1} in the UTD-1_{faulted} spectrum can also be observed, which is not present for UTD-1_{faultless} and is associated with framework defects or Si–OH from siloxy groups.^{67,68} Fig. 5 shows FTIR spectra for the variants after adsorption of TMS (*i.e.*, TMS@UTD-1_{faulted} and TMS@UTD-1_{faultless}). For UTD-1_{faulted}, it can be observed that there is a new band at 850 cm^{−1}. This could be related to Si–CH₃

bonds stretching in the TMS molecules or to the Si–O–Si bending mode of weak bonds created by the interaction between TMS and the adsorbent surface, or plausibly due to the deformations of the Si–OH groups of TMS. An important fact from the TMS@UTD-1_{faulted} spectrum is the absence of the band related to faults (*i.e.*, band at 950 cm^{−1} in fresh UTD-1_{faulted}). This probably reinforces the hypothesis that the presence of OH groups on the surface of the adsorbent serves as site for the adsorption of the TMS.

The IR spectrum for TMS@UTD-1_{faultless} exhibits changes within the region between 850 and 1000 cm^{−1} relative to the spectrum of fresh material. This could be attributed to the adsorbed TMS phase, which introduces OH groups. Such a change is entirely distinct from that observed in the faulted material, and this provides further support for the previously proposed mechanism of TMS adsorption in UTD-1_{faulted}.

Multi-components adsorption

Evaluation of multi-component siloxane adsorption (*i.e.*, simultaneous adsorption of a mixture of siloxanes) onto either UTD-1 variant was carried out *via* single-point batch equilibration tests at two different initial concentrations. The aqueous phase solutions were prepared with an initial concentration of *ca.* 1 and 10 mg of organic carbon per liter of solution (*i.e.*, 1 and 10 mg C per L) of each contaminant at ambient temperature and pH \sim 7. From Fig. 6, although the UTD-1 variants show poor performance at 1 mg C per L regarding the binary DMSD–

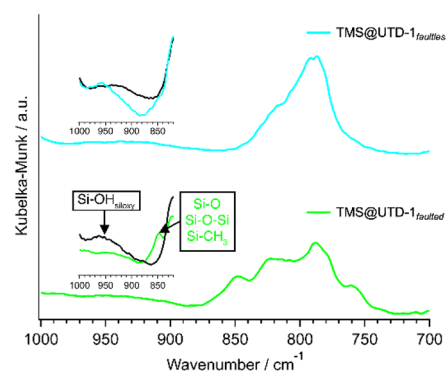


Fig. 5 FTIR spectra UTD-1 variants after TMS adsorption. Inset shows magnified portions of distinctive peaks found in the FTIR spectra. The solid black line data corresponding to the fresh adsorbent (Fig. S5†) spectrum have been included for better comparison.



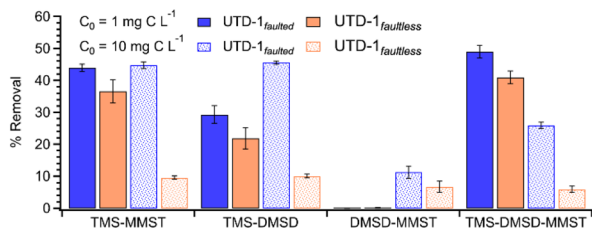


Fig. 6 Single point binary and ternary (far right) mixtures equilibrium uptakes for different siloxanes onto both UTD-1 variants. Conditions: the initial concentration of each contaminant was 1 and 10 mg C per L (*i.e.*, ppm C), ambient temperature, and pH ~ 7 .

MMST adsorption, the adsorbents excelled for other binary combinations or ternary systems. However, from the adsorption results at 10 mg C per L, it is evident that UTD-1_{faulted} is superior when handling ternary mixtures. These findings are also consistent with those in the single-component adsorption tests (see Fig. 4), where the adsorbents exhibit similar behavior at low concentrations, such as 1 mg C per L. Still, the adsorption capacity shown by UTD-1_{faulted} at higher concentrations is superior.

A notable aspect that should be highlighted is that TMS appears to be the main driving force for the adsorption of the other two compounds. In the case of binary mixtures (Fig. 6, left), it is difficult to elucidate how much of the adsorbed amount corresponds to TMS *versus* the other contaminant (*i.e.*, the initial concentration of each adsorbate is 1 or 10 mg C per L). However, TMS positively affects the adsorption of other siloxanes and is the main contributor to the substantial uptakes; evidencing co-adsorption may be due to strong adsorbate–adsorbate interactions between TMS and other siloxanes.

Adsorbent regeneration

Tests with batch equilibrium adsorption of TMS onto UTD-1_{faulted} were chosen for adsorbent regeneration tests since this adsorbate–adsorbent system showed the highest interactions. As mentioned before, PSZs like UTD-1 have demonstrated exceptional thermal stability, making them suitable for thermal-based regeneration processes,⁵² and offering an advantage for the removal of adsorbent pollutants on spent UTD-1; which requires activation temperatures of around 700 °C (see Fig. S6† for thermogravimetric data). However, since the hydroxyl groups on the adsorbent surface promote the adsorption of contaminants such as TMS, which are also removed at temperatures higher than 500 °C, surface OH replenishment can be accomplished *via* rehydroxylation.⁶⁹

Restoring hydroxyls on the adsorbent surface through exposure to water refluxing was a successful process in recovering the capability of UTD-1_{faulted} to adsorb TMS. Fig. 7 shows the adsorbent amount of TMS after multiple cycles (*i.e.*, regeneration or rejuvenation of the adsorbent *via* thermal treatment and rehydroxylation). The efficiency of the adsorbent material remains constant even up to at least a third adsorption cycle, and the integrity of the material is not affected, as shown in the

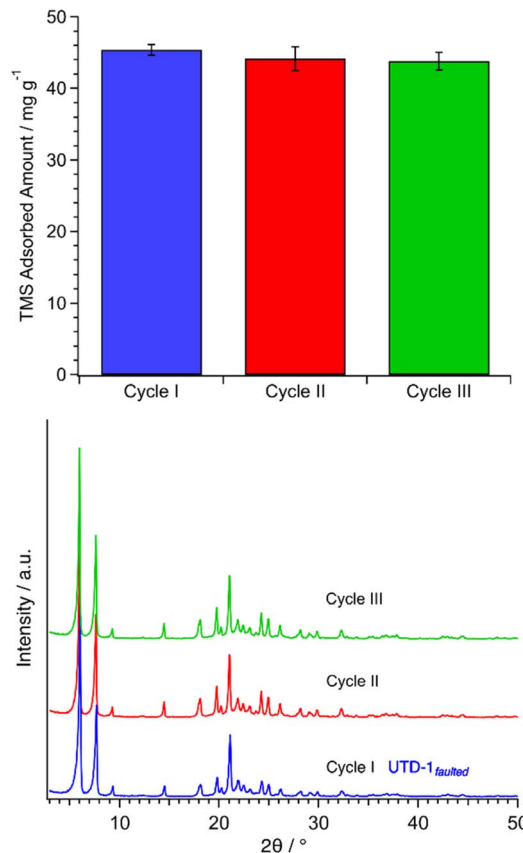


Fig. 7 (Top) Adsorbed amount of TMS onto fresh and regenerated UTD-1_{faulted}. (Bottom) XRD pattern of UTD-1_{faulted} prior to each adsorption cycle. The initial TMS concentration during the adsorption tests was 125 mg L⁻¹. Adsorbent regeneration was performed through thermal treatment and rehydroxylation.

XRD profiles. A two-cycle test was performed for attempting the regeneration of UTD-1_{faulted} upon being spent with the adsorption of a ternary mixture of siloxanes (TMS–DMSD–MMST) (see Fig. S7†). The results match those observed for the single-component (TMS) tests in terms of capacity and long-range adsorbent integrity.

Conclusions

The faults in the PSZ UTD-1 play an essential role in the uptake of the siloxanes from water, particularly TMS, since the target molecules could interact with the silanol groups from the surface. The interaction mechanism for DMSD appears to be *via* weak electrostatic forces. In the case of TMS, the uptake in UTD-1_{faulted} was the highest and exhibited a nearly rectangular isotherm shape across the evaluated equilibrium concentration range (up to 150 mg L⁻¹). The silanol content due to siloxy faults in the UTD-1_{faulted} surface is the dominant driving force in the uptake of siloxanes such as TMS, which was confirmed by FTIR. A faultless adsorbent variant (UTD-1_{faultless}) shows lower interaction with TMS as it does not contain silanol groups from siloxy faults. Furthermore, multi-component adsorption tests revealed that TMS drives the co-adsorption of the other siloxane



compounds when in a mixture. Finally, the recyclability of UTD-1_{faulted} was corroborated based on multi-cycle TMS adsorption tests; the adsorbent was successfully regenerated between cycles using thermal and rehydroxylation treatments.

Author contributions

Dariana Vega-Santander: conceptualization, methodology, investigation, formal analysis, writing – original draft. Rodinson Arrieta-Perez: investigation, formal analysis. Daniela Rivera-Mirabal: investigation, formal analysis. Gabriela Del Valle-Pérez: investigation, formal analysis. Miguel Sepúlveda-Pagán: investigation, formal analysis. Juan C. Muñoz-Senmache: investigation, formal analysis, writing – original draft. Yomaira J. Pagán-Torres: methodology, investigation, formal analysis, writing – original draft. Arturo J. Hernandez-Maldonado: conceptualization, methodology, investigation, formal analysis, writing – review & editing, visualization, project administration, funding acquisition.

Conflicts of interest

There are no conflicts to declare.

Acknowledgements

This work was supported by the US National Aeronautics and Space Administration (NASA) – NASA MIRO-Puerto Rico Space Partnership for Research, Education, and Training (PRSPRInT) grant no. 80NSSC19M0236.

References

- 1 M. Pedrouzo, F. Borrell, R. M. Marcé and E. Pocurull, Analytical methods for personal-care products in environmental waters, *Trends Anal. Chem.*, 2011, **30**, 749–760.
- 2 L. Zhi, L. Xu, X. He, C. Zhang and Y. Cai, Occurrence and profiles of methylsiloxanes and their hydrolysis product in aqueous matrices from the Daqing oilfield in China, *Sci. Total Environ.*, 2018, **631**, 879–886.
- 3 J. Velicogna, E. Ritchie, J. Princz, M.-E. Lessard and R. Scroggins, Ecotoxicity of siloxane D5 in soil, *Chemosphere*, 2012, **87**, 77–83.
- 4 C. Rauert, T. Harner, J. K. Schuster, A. Eng, G. Fillmann, L. E. Castillo, O. Fentanes, M. N. V. Ibarra, K. S. Miglioranza and I. M. Rivadeneira, Atmospheric concentrations of new persistent organic pollutants and emerging chemicals of concern in the group of latin america and caribbean (GRULAC) region, *Environ. Sci. Technol.*, 2018, **52**, 7240–7249.
- 5 X. Xiang, N. Liu, L. Xu and Y. Cai, Review of recent findings on occurrence and fates of siloxanes in environmental compartments, *Ecotoxicol. Environ. Saf.*, 2021, **224**, 112631.
- 6 F. Bernardo, A. Alves and V. Homem, A review of bioaccumulation of volatile methylsiloxanes in aquatic ecosystems, *Sci. Total Environ.*, 2022, **824**, 153821.
- 7 *Silicones and Siloxanes Market: Global Industry Trends, Share, Size, Growth, Opportunity and Forecast 2023–2028*, IMARC Group, 2023.
- 8 M. W. Alton and E. C. Browne, Atmospheric chemistry of volatile methyl siloxanes: kinetics and products of oxidation by OH radicals and Cl atoms, *Environ. Sci. Technol.*, 2020, **54**, 5992–5999.
- 9 K. Mojsiewicz-Pieńkowska and D. Krenczkowska, Evolution of consciousness of exposure to siloxanes—review of publications, *Chemosphere*, 2018, **191**, 204–217.
- 10 S. Lee, H.-B. Moon, G.-J. Song, K. Ra, W.-C. Lee and K. Kannan, A nationwide survey and emission estimates of cyclic and linear siloxanes through sludge from wastewater treatment plants in Korea, *Sci. Total Environ.*, 2014, **497–498**, 106–112.
- 11 J. Sanchís, A. Cabrerizo, C. Galbán-Malagón, D. Barceló, M. Farré and J. Dachs, Unexpected occurrence of volatile dimethylsiloxanes in Antarctic soils, vegetation, phytoplankton, and krill, *Environ. Sci. Technol.*, 2015, **49**, 4415–4424.
- 12 L. Xu, S. Xu, L. Zhi, X. He, C. Zhang and Y. Cai, Methylsiloxanes release from one landfill through yearly cycle and their removal mechanisms (especially hydroxylation) in leachates, *Environ. Sci. Technol.*, 2017, **51**, 12337–12346.
- 13 M. M. Coggon, B. C. McDonald, A. Vlasenko, P. R. Veres, F. o. Bernard, A. R. Koss, B. Yuan, J. B. Gilman, J. Peischl and K. C. Aikin, Diurnal variability and emission pattern of decamethylcyclopentasiloxane (D5) from the application of personal care products in two North American cities, *Environ. Sci. Technol.*, 2018, **52**, 5610–5618.
- 14 S.-Y. Lee, S. Lee, M. Choi, K. Kannan and H.-B. Moon, An optimized method for the analysis of cyclic and linear siloxanes and their distribution in surface and core sediments from industrialized bays in Korea, *Environ. Pollut.*, 2018, **236**, 111–118.
- 15 X. Wang, J. Schuster, K. C. Jones and P. Gong, Occurrence and spatial distribution of neutral perfluoroalkyl substances and cyclic volatile methylsiloxanes in the atmosphere of the Tibetan Plateau, *Atmos. Chem. Phys.*, 2018, **18**, 8745–8755.
- 16 L. Zhi, L. Xu, Y. Qu, C. Zhang, D. Cao and Y. Cai, Identification and elimination of fluorinated methylsiloxanes in environmental matrices near a manufacturing plant in eastern China, *Environ. Sci. Technol.*, 2018, **52**, 12235–12243.
- 17 E. C. Tuazon, S. M. Aschmann and R. Atkinson, Atmospheric degradation of volatile methyl-silicon compounds, *Environ. Sci. Technol.*, 2000, **34**, 1970–1976.
- 18 J. A. Rutz, J. R. Schultz, C. M. Kuo, H. E. Cole, S. Manuel, M. Curtis, P. R. Jones, O. D. Sparkman and J. T. McCoy, Presented in Part at the 41st International Conference on Environmental Systems, Portland, Oregon, 2011.
- 19 T. Rector, C. Metselaar, B. Peyton, J. Steele, W. Michalek, E. Bowman, M. Wilson, D. Gazda and L. Carter, Presented in Part at the 44th International Conference on Environmental Systems, Tucson, Arizona, 13–17 July, 2014.



- 20 R. Amanathan, J. Ames and T. McCoy, Acceptable levels for ingestion of dimethylsilanediol in water on the International Space Station, *Aviat., Space Environ. Med.*, 2012, **83**, 598–603.
- 21 J. T. James, in *Spacecraft Maximum Allowable Concentrations for Selected Airborne Contaminants*, The National Academies Press, Washington, DC, 2008, DOI: [10.17226/12529](https://doi.org/10.17226/12529).
- 22 J. V. Sousa, P. C. McNamara, A. E. Putt, M. W. Machado, D. C. Surprenant, J. L. Hamelink, D. J. Kent, E. M. Silberhorn and J. F. Hobson, Effects of octamethylcyclotetrasiloxane (OMCTS) on freshwater and marine organisms, *Environ. Toxicol. Chem.*, 1995, **14**, 1639–1647.
- 23 L. Carter, J. Perry, M. J. Kayatin, M. Wilson, G. J. Gentry, E. Bowman, O. Monje, T. Rector and J. Steele, *Presented in Part at the 45th International Conference on Environmental Systems*, Bellevue, Washington, 12–16 July, 2015.
- 24 L. Carter, J. Pruitt, C. A. Brown, R. Schaezler and L. Bankers, *Presented in Part at the 45th International Conference on Environmental Systems*, Bellevue, Washington, 12–16 July, 2015.
- 25 S. Liu, B. Chen, Y. Yang, Y. Yang, Q. Chen, X. Zeng and B. Xu, Electrochemical oxidations of thioethers: modulation of oxidation potential using a hydrogen bonding network, *Electrochem. Commun.*, 2019, **109**, 106583.
- 26 M. Ajhar, M. Travesset, S. Yüce and T. Melin, Siloxane removal from landfill and digester gas—a technology overview, *Bioresour. Technol.*, 2010, **101**, 2913–2923.
- 27 A. Cabrera-Codony, M. A. Montes-Morán, M. Sánchez-Polo, M. J. Martín and R. Gonzalez-Olmos, Biogas upgrading: optimal activated carbon properties for siloxane removal, *Environ. Sci. Technol.*, 2014, **48**, 7187–7195.
- 28 D.-G. Wang, M. Aggarwal, T. Tait, S. Brimble, G. Pacepavicius, L. Kinsman, M. Theocharides, S. A. Smyth and M. Alaei, Fate of anthropogenic cyclic volatile methylsiloxanes in a wastewater treatment plant, *Water Res.*, 2015, **72**, 209–217.
- 29 V. T. L. Tran, P. Gélín, C. Ferronato, P. Mascunan, V. Rac, J.-M. Chovelon and G. Postole, Siloxane adsorption on activated carbons: role of the surface chemistry on sorption properties in humid atmosphere and regenerability issues, *Chem. Eng. J.*, 2019, **371**, 821–832.
- 30 D. R. Ortega and A. Subrenat, Siloxane treatment by adsorption into porous materials, *Environ. Technol.*, 2009, **30**, 1073–1083.
- 31 D. R. Vega-Santander, J. C. Muñoz-Senmache, J. Borrero-Negrón, Y. J. Pagán-Torres and A. J. Hernández-Maldonado, Removal of linear siloxanes and dimethyl sulfone from water using hierarchical zeolite porous carbon adsorbents, *J. Hazard. Mater.*, 2022, **440**, 129805.
- 32 S. Li, X. Wang, D. Beving, Z. Chen and Y. Yan, Molecular sieving in a nanoporous b-oriented pure-silica-zeolite MFI monocystal film, *J. Am. Chem. Soc.*, 2004, **126**, 4122–4123.
- 33 D. S. Wragg, R. E. Morris and A. W. Burton, Pure silica zeolite-type frameworks: a structural analysis, *Chem. Mater.*, 2008, **20**, 1561–1570.
- 34 J. C. Muñoz-Senmache, B. Fernández-Reyes and A. J. Hernández-Maldonado, Progress in the design of nanoporous adsorbent materials containing transition metals for the removal of contaminants of emerging concern, *Environ. Pollut. Bioavailability*, 2021, **33**, 41–54.
- 35 I. Ahmed and S. H. Jung, Composites of metal–organic frameworks: preparation and application in adsorption, *Mater. Today*, 2014, **17**, 136–146.
- 36 J. C. Muñoz-Senmache, S. Kim, R. R. Arrieta-Pérez, C. M. Park, Y. Yoon and A. J. Hernández-Maldonado, Activated carbon–metal organic framework composite for the adsorption of contaminants of emerging concern from water, *ACS Appl. Nano Mater.*, 2020, **3**, 2928–2940.
- 37 J. C. Muñoz-Senmache, P. E. Cruz-Tato, E. Nicolau and A. J. Hernández-Maldonado, Confined space synthesis of chromium–based metal–organic frameworks in activated carbon: synergistic effect on the adsorption of contaminants of emerging concern from water, *J. Environ. Chem. Eng.*, 2022, **10**, 107282.
- 38 N. Jiang, R. Shang, S. G. J. Heijman and L. C. Rietveld, High-silica zeolites for adsorption of organic micro-pollutants in water treatment: a review, *Water Res.*, 2018, **144**, 145–161.
- 39 M. Khalid, G. Joly, A. Renaud and P. Magnoux, Removal of phenol from water by adsorption using zeolites, *Ind. Eng. Chem. Res.*, 2004, **43**, 5275–5280.
- 40 M. Miyamoto, S. Ono, K. Kusukami, Y. Oumi and S. Uemiyama, High water tolerance of a core-shell-structured zeolite for CO₂ adsorptive separation under wet conditions, *ChemSusChem*, 2018, **11**, 1756–1760.
- 41 H. Abdi and H. Maghsoudi, All-silica DD3R zeolite for adsorptive separation of propylene from propane: equilibrium and kinetic data, *Microporous Mesoporous Mater.*, 2020, **307**, 110513.
- 42 E. Pérez-Botella, A. Misturini, A. Sala, M. Palomino, A. Corma, G. Sastre, S. Valencia and F. Rey, Insights into adsorption of linear, monobranched, and dibranched alkanes on pure silica STW zeolite as a promising material for their separation, *J. Phys. Chem. C*, 2020, **124**, 26821–26829.
- 43 J. Wang, C. Ma, J. Liu, Y. Liu, X. Xu, M. Xie, H. Wang, L. Wang, P. Guo and Z. Liu, Pure silica with ordered silanols for propylene/propane adsorptive separation unraveled by three-dimensional electron diffraction, *J. Am. Chem. Soc.*, 2023, **145**, 6853–6860.
- 44 T. C. Bowen and L. M. Vane, Ethanol, acetic acid, and water adsorption from binary and ternary liquid mixtures on high-silica zeolites, *Langmuir*, 2006, **22**, 3721–3727.
- 45 J. Reungoat, J. S. Pic, M. H. Manéro and H. Debellefontaine, Adsorption of nitrobenzene from water onto high silica zeolites and regeneration by ozone, *Sep. Sci. Technol.*, 2007, **42**, 1447–1463.
- 46 N. Jiang, R. Shang, S. G. J. Heijman and L. C. Rietveld, Adsorption of triclosan, trichlorophenol and phenol by high-silica zeolites: adsorption efficiencies and mechanisms, *Sep. Purif. Technol.*, 2020, **235**, 116152.
- 47 S. Lin, Y. Wang, Y. Zhao, L. Pericchi, A. J. Hernandez-Maldonado and Z. Chen, Machine-learning-assisted



- screening of pure-silica zeolites for effective removal of linear siloxanes and derivatives, *J. Mater. Chem. A*, 2020, **8**, 3228–3237.
- 48 I. C. Medeiros-Costa, E. Dib, N. Nesterenko, J.-P. Dath, J.-P. Gilson and S. Mintova, Silanol defect engineering and healing in zeolites: opportunities to fine-tune their properties and performances, *Chem. Soc. Rev.*, 2021, **50**, 11156–11179.
 - 49 T. Wessels, C. Baerlocher, L. B. McCusker and E. J. Creghton, An ordered form of the extra-large-pore zeolite UTD-1: synthesis and structure analysis from powder diffraction data, *J. Am. Chem. Soc.*, 1999, **121**, 6242–6247.
 - 50 M. S. Nabavi, M. Zhou, J. Mouzon, M. Grahn and J. Hedlund, Stability of colloidal ZSM-5 catalysts synthesized in fluoride and hydroxide media, *Microporous Mesoporous Mater.*, 2019, **278**, 167–174.
 - 51 C. C. Freyhardt, M. Tsapatsis, R. F. Lobo, K. J. Balkus and M. E. Davis, A high-silica zeolite with a 14-tetrahedral-atom pore opening, *Nature*, 1996, **381**, 295–298.
 - 52 R. F. Lobo, M. Tsapatsis, C. C. Freyhardt, S. Khodabandeh, P. Wagner, C.-Y. Chen, K. J. Balkus, S. I. Zones and M. E. Davis, Characterization of the extra-large-pore zeolite UTD-1, *J. Am. Chem. Soc.*, 1997, **119**, 8474–8484.
 - 53 H. Zhang, G. X. Li, J. X. Zhang, D. L. Zhang, Z. Chen, X. N. Liu, P. Guo, Y. H. Zhu, C. L. Chen, L. M. Liu, X. W. Guo and Y. Han, Three-dimensional inhomogeneity of zeolite structure and composition revealed by electron ptychography, *Science*, 2023, **380**, 633–638.
 - 54 K. Balkus and S. Shepelev, Synthesis of nonasil molecular sieves in the presence of cobalticinium hydroxide, *Microporous Mater.*, 1993, **1**, 383–400.
 - 55 G. Chandra, *Organosilicon Materials*, Springer, 1997.
 - 56 S. Xu and B. Kropscott, Method for simultaneous determination of partition coefficients for cyclic volatile methylsiloxanes and dimethylsilanediol, *Anal. Chem.*, 2012, **84**, 1948–1955.
 - 57 S. Xu and B. Kropscott, Evaluation of the three-phase equilibrium method for measuring temperature dependence of internally consistent partition coefficients (KOW, KOA, and KAW) for volatile methylsiloxanes and trimethylsilanol, *Environ. Toxicol. Chem.*, 2014, **33**, 2702–2710.
 - 58 T. D. Pham, R. Xiong, S. I. Sandler and R. F. Lobo, Experimental and computational studies on the adsorption of CO₂ and N₂ on pure silica zeolites, *Microporous Mesoporous Mater.*, 2014, **185**, 157–166.
 - 59 R. F. Lobo, S. I. Zones and M. E. Davis, Structure-direction in zeolite synthesis, *J. Inclusion Phenom. Mol. Recognit. Chem.*, 1995, **21**, 47–78.
 - 60 H. Koller, R. F. Lobo, S. L. Burkett and M. E. Davis, SiO₄–HOSi hydrogen bonds in as-synthesized high-silica zeolites, *J. Phys. Chem.*, 1995, **99**, 12588–12596.
 - 61 K. J. Balkus, M. Biscotto and A. G. Gabrielov, in *Stud. Surf. Sci. Catal.*, ed. H. Chon, S.-K. Ihm and Y. S. Uh, Elsevier, 1997, vol. 105, pp. 415–421.
 - 62 Y. Wei, Z. J. Tian, H. Gies, R. S. Xu, H. J. Ma, R. Y. Pei, W. P. Zhang, Y. P. Xu, L. Wang, K. D. Li, B. C. Wang, G. D. Wen and L. W. Lin, Ionothermal Synthesis of an Aluminophosphate Molecular Sieve with 20-Ring Pore Openings, *Angew. Chem., Int. Ed.*, 2010, **49**, 5367–5370.
 - 63 C. M. Zicovich-Wilson, M. L. San Román and A. Ramírez-Solís, Mechanism of F[−] elimination from zeolitic D4R units: a periodic B3LYP study on the octadecasil zeolite, *J. Phys. Chem. C*, 2010, **114**, 2989–2995.
 - 64 D. P. Serrano, R. Van Grieken, P. Sánchez, R. Sanz and L. Rodríguez, Crystallization mechanism of all-silica zeolite beta in fluoride medium, *Microporous Mesoporous Mater.*, 2001, **46**, 35–46.
 - 65 K. Hadjiivanov, in *Advances in Catalysis*, ed. F. C. Jentoft, Academic Press, 2014, vol. 57, pp. 99–318.
 - 66 H. Jung and J. Jurng, Purification of wastewater digester biogas from siloxanes via adsorption-desorption with NaOH-reformed SiO₂ adsorbent, *Renewable Energy*, 2020, **156**, 459–468.
 - 67 K. J. Balkus, A. G. Gabrielov and S. I. Zones, in *Stud. Surf. Sci. Catal.*, ed. L. Bonnevot and S. Kaliaguine, Elsevier, 1995, vol. 97, pp. 519–525.
 - 68 T. Muñoz and K. J. Balkus, Preparation of oriented zeolite UTD-1 membranes via pulsed laser ablation, *J. Am. Chem. Soc.*, 1999, **121**, 139–146.
 - 69 S. Shioji, M. Kawaguchi, Y. Hayashi, K. Tokami and H. Yamamoto, Rehydroxylation of dehydrated silica surfaces by water vapor adsorption, *Adv. Powder Technol.*, 2001, **12**, 331–342.

